WHITE PAPER | 2020

CPAS
ClusterTech

www.cpas.earth

Evaluation of Mesh Quality, Run-time Efficiency, and Predictability for CPAS Customized Variable-Resolution Mesh

聯科集團
CLUSTERTECH

Cloud + High Performance Computing + AI & Analytics + Big Data
Business Intelligence · Financial Engineering · Environmental Science · Smart City

www.clustertech.com

Hong Kong · Beijing · Shanghai · Guangzhou · Shenzhen · Xi'an · Sydney

Abstract

The ClusterTech Platform for Atmospheric Simulation (CPAS) consists of two innovations. First, the Customizable Unstructured Mesh Generation (CUMG) enables local mesh refinement in arbitrary shape using user-defined horizontal resolution in any desired locations. Generation of meshes with large resolution variation for high resolution regional forecast becomes possible. Second, to save computational resources in time-integration on such meshes, different time-steps are applied to mesh cells of different sizes using Hierarchical Time-Stepping (HTS). This reduces the model run time tremendously for meshes with large resolution variation. This study compares the mesh quality, real simulation efficiency, as well as predictive performance of a CPAS customized 128-to-1 km mesh to the Model for Prediction Across Scales - Atmosphere (MPAS-A) standard 60-to-3 km mesh by simulating three historical scenarios, with and without HTS.

The CPAS 128-to-1 km mesh was found to have better quality over the MPAS-A 60-to-3 km mesh, namely cell quality, angle-based triangle quality, and triangle quality. Using HTS, the benchmarked saving of the total run time for the CPAS 128-to-1 km mesh and MPAS-A 60-to-3 km mesh are 56.8% (2.33x speedup) and 16.5% (1.20x speedup) respectively. By comparing the 5-day simulation results with the National Centers for Environmental Prediction (NCEP) Final (FNL) Operational Global Analysis, all forecast variables show comparable performance in all cases with and without HTS for both customized and standard meshes, illustrating the validity of the CPAS customized mesh running in HTS. On comparing with daily mean temperature measured by 28 local weather stations operated by the Hong Kong Observatory (HKO), the CPAS 128-to-1 km mesh generally produces higher correlation coefficient than the standard 60-to-3 km mesh in all cases. The promising model performance along with remarkable speedup indicates the validity and feasibility of using meshes with large resolution variation for local/regional forecast in operational manner.

1. Introduction

The model performance and model run time are two major concerns for atmospheric simulation. Both are substantially dependent on the mesh specification, in particular, the number of mesh cells, mesh resolutions and coverage of the refinement regions. In MPAS-A, a globally-constant time-step (determined by the CFL condition of the smallest grid) is used. This however, poses challenges on high resolution regional forecast using meshes with large resolution variation due to impractically long run time.

In CPAS, CUMG is an in-house implementation based on, or strongly influenced, by several literatures [1–6]. The unstructured grid mainly consists of hexagonal cells, with a few pentagons and heptagons. The corresponding dual Delaunay triangular mesh is guaranteed to have no obtuse triangle and hence never off-centred. Following a bisection refinement algorithm[1], the construction of grid connectivity for CPAS's mesh with local refinement is non-iterative, and the mesh quality are then enhanced through optimization iterations without breaking the connectivity. This results in extremely fast grid convergence in mesh generation [1–3]. Furthermore, for simulations using variable-resolution meshes, the restriction on using a globally-constant time-step is relaxed by HTS. It applies different time-steps to mesh cells of different sizes, therefore a more efficient utilization of computational resources can be achieved.

This study evaluates the mesh quality, run-time efficiency, and predictability of a CPAS customized 128-to-1 km mesh with comparison to the MPAS-A standard 60-to-3 km mesh with and without HTS. Three cases occurred in 2018 were chosen, namely, passage of a cold front (Case 1), heavy rainfall associated with a trough of low pressure (Case 2), and passage of a tropical cyclone (Case 3).

2. MPAS-A Standard 60-to-3 km Mesh vs CPAS Customized 128-to-1 km Mesh

The two meshes differ from the shape, span and number of refinement regions, and range of resolution variations as shown in Fig. 1 and Fig. 2. Specifically, the standard 60-to-3 km mesh contains 835,586 horizontal grid cells with a circular refinement region, while the customized 128-to-1 km mesh contains 126,515 horizontal grid cells with several arbitrary-shaped refinement regions.

The 128-to-1 km mesh was tailor made for weather forecast over Hong Kong and the coastal area of Guangdong province. It was generated using 500 optimization iterations, with roughly 1-km resolution covering Hong Kong and its adjacent waters. The center of the refinement region of the 60-to-3 km mesh was relocated to Hong Kong.

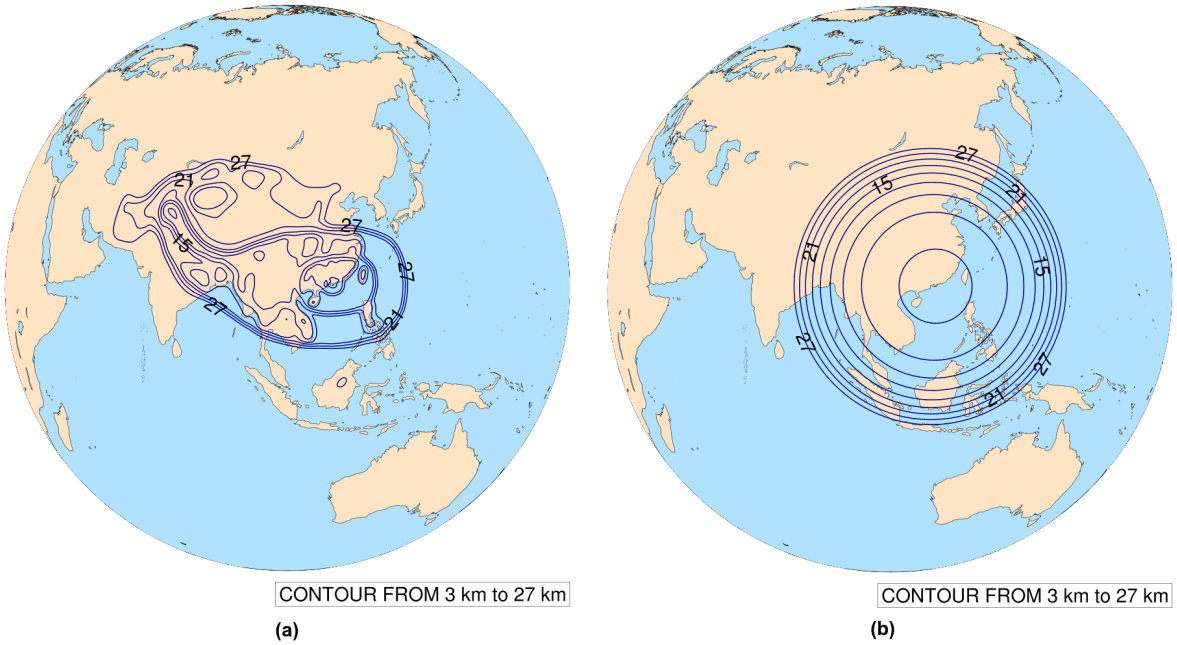

Figure 1: Mesh resolution drawn on orthographic projection maps centered on 10° N, 105.0° E for (a) the customized 128-to-1 km mesh and (b) the standard 60-to-3 km mesh

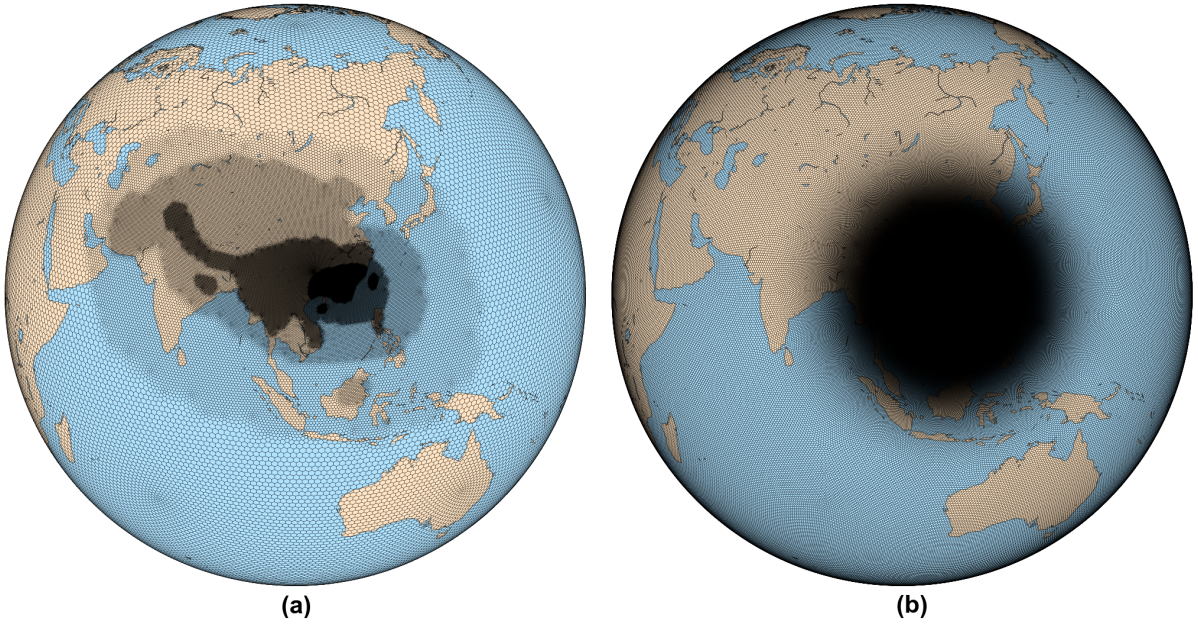

Figure 2: Voronoi mesh drawn on orthographic projection maps centered on 10° N, 105.0° E for (a) customized 128-to-1 km mesh and (b) the standard 60-to-3 km mesh. Darker refined regions infer their finer resolution

A. Mesh quality

The mesh quality can be determined by four quality parameters – cell quality (regularity of the mesh cell), angle based triangle quality (regularity of the interior angles of the dual), triangle quality (regularity of the edges of the dual), and number of obtuse triangles of the dual.

Denote the length of an edge of the Voronoi cell as l, cell quality is determined by the quotient of the shortest and longest edges of the cell:

$$\text{Cell Quality} = \frac{l_{\text{min}}}{l_{\text{max}}} \tag{1}$$

Consider the dual (Delaunay triangulation) of the Voronoi cell, denote the interior angle as θ, and the edges as a, b and c. The angle-based triangle quality and triangle quality are determined by Eq. (2) and Eq. (3) respectively:

$$\text{Angle-Based Triangle Quality} = \frac{\theta_{\text{min}}}{\theta_{\text{max}}} \tag{2}$$

$$\text{Triangle Quality} = \frac{(a+b-c)(b+c-a)(a+c-b)}{abc} \tag{3}$$

It is perfect to have these three qualities equal to 1, and the number of obtuse triangles equal to 0. However, to generate a variable-resolution mesh, a certain number of stretched cells must exist. A high quality mesh should contain a large number of cells having qualities close to 1, while the minimum of the qualities are sufficiently high to maintain numerical stability.

It is discovered that both meshes have zero obtuse triangle. Moreover, refer to the distribution of mesh qualities in Fig. 3, the CPAS 128-to-1 km mesh (blue) has an overall better quality than the MPAS-A 60-to-3 km mesh (yellow) for both the mean (solid line) and minimum (dashed line), showing the feasibility of CUMG algorithm for generating meshes with large resolution variation.

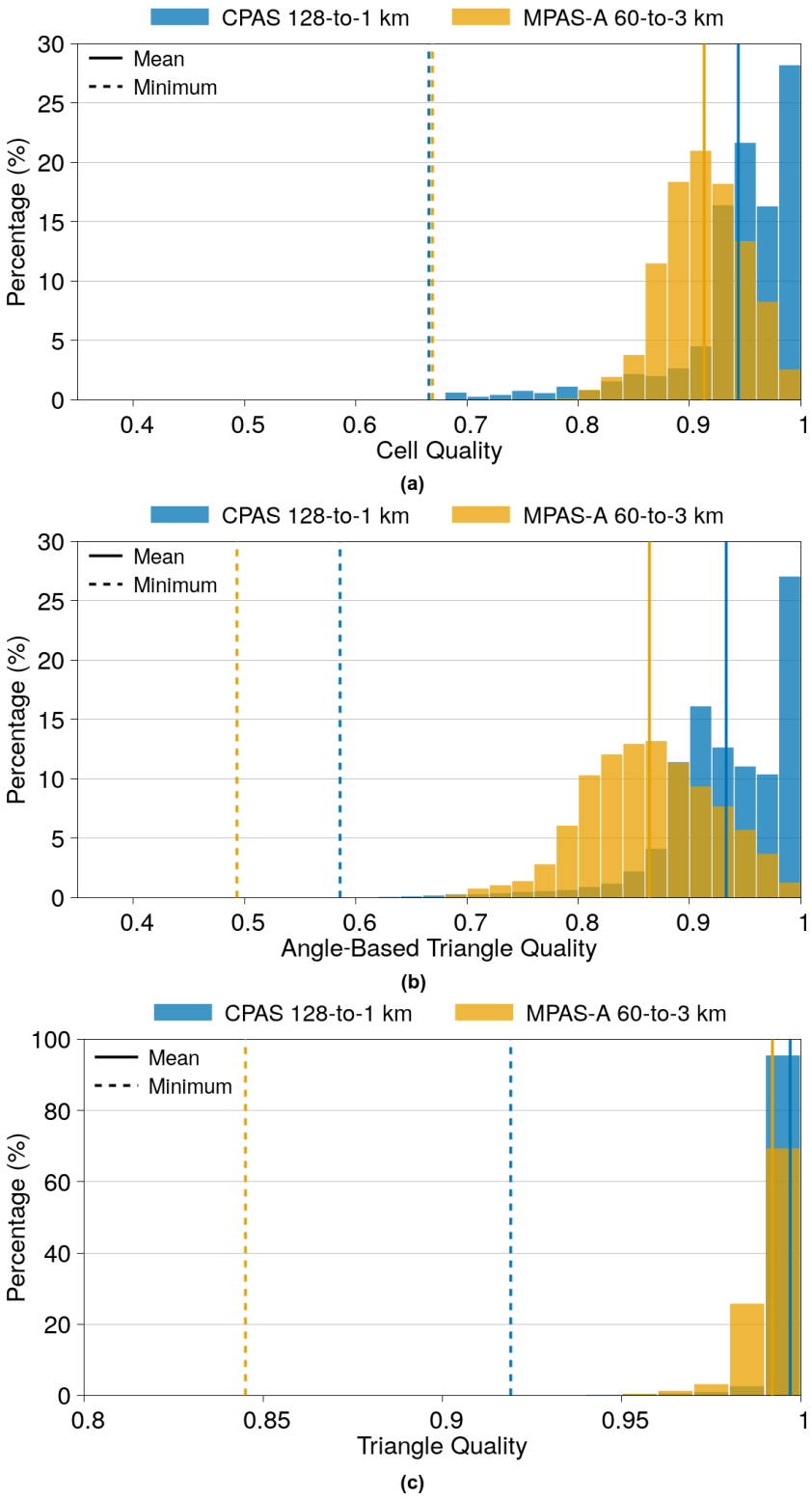

Figure 3: Distribution of the mesh qualities for the customized 128-to-1 km mesh (blue) and the standard 60-to-3 km mesh (yellow): (a) cell quality (b) angle-based triangle quality (c) triangle quality

B. HTS levels assignment

The HTS level (n) is a non-negative integer assigning on each mesh cell (including halo cells [7]) based on its horizontal resolution. Fig. 4 shows the spatial distribution of the HTS levels assigned on mesh cells in the two global SCVTs. The smaller the mesh cells, the higher the HTS levels, and the smaller the time-step used during model integration.

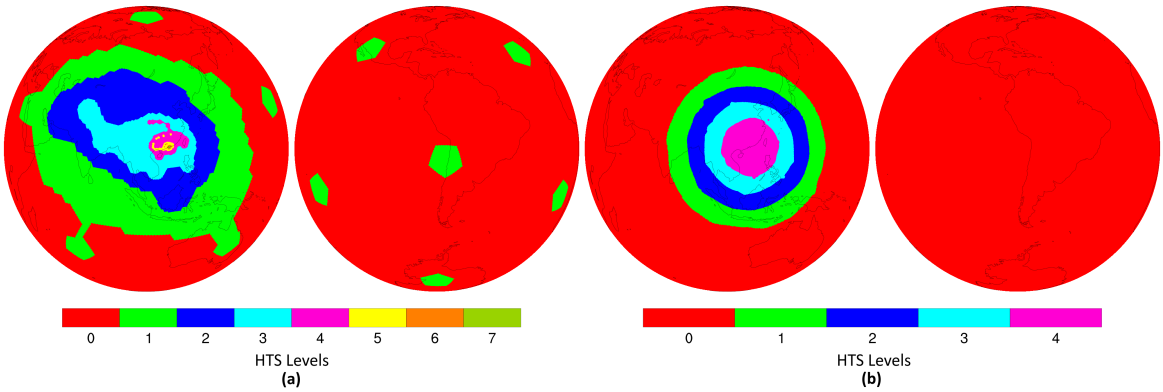

Figure 4: Spatial distribution of the HTS levels assigned on (a) the customized 128-to-1 km mesh and (b) the standard 60-to-3 km mesh drawn on orthographic projection maps centered on 10° N, 105.0° E (left) and 10.0° S, 75.0° W (right)

Based on Fig. 4, the summary of resolutions, time-steps, total number and percentage of cells, and time saving when compared with MPAS-A are tabulated in Fig. 5. Denote the largest time-step (smallest HTS level) as dt_0, then the time-step for HTS level n were determined by:

$$dt_n = 2^{-n} dt_0 \tag{4}$$

For non-HTS cases, the time-step were set to be equivalent to the time-step of the largest HTS level, i.e. 9.375 s (dt_4) for the standard 60-to-3 km mesh and 2.34375 s (dt_7) for the customized 128-to-1 km mesh. These values are roughly equals to 4 times of the actual minimum grid spacing in kilometers: 2.38 km (the standard 60-to-3 km mesh) and 0.591 km (the customized 128-to-1 km mesh). It is noted that the time saving is a theoretically estimated value by assuming perfect scalability of inter-process communications, perfect threading optimization, and negligible input/output time.

The HTS tables in Fig. 5 can be represented by variable width column charts shown in Fig. 6, where the y- and x-axis refer to relative resource usage and percentage of cells respectively. Suppose the resource usage of MPAS-A (i.e. without HTS) is indicated by the area under the 100% resource usage because a globally-constant time-step is used for all cells. In CPAS (i.e. with HTS), the resource usage for cells of different sizes are different, which are illustrated by the green bars (HTS levels ascending from left to right). And the area emerging the resource usage of MPAS-A, i.e. area enclosed by the orange rectangle, is the overhead. Therefore, the overall resource saved by HTS is the difference of red region and orange rectangle.

Hierarchical Time-stepping by ClusterTech

Table | Chart | Segments

Level	Resolution distance between cells	Time step	#Cell (%)	CPU core resource in giga cell-step per simulation day (%)	Saving
0	109.066km - 135.846km	300.000s	28,423 (22.47%)	0.01 (0.93%)	99.15%
1	45.169km - 138.798km	150.000s	8,892 (7.03%)	0.01 (1.05%)	96.97%
2	21.011km - 98.640km	75.000s	16208 (12.81%)	0.03 (2.58%)	95.90%
3	9.761km - 34.413km	37.500s	31,399 (24.82%)	0.12 (9.23%)	92.44%
4	4.806km - 28.253km	18.750s	19,461 (15.38%)	0.16 (12.65%)	83.27%
5	2.389km - 13.753km	9.375s	8,561 (6.77%)	0.18 (14.54%)	56.32%
6	1.191km - 6.924km	4.6875s	3,989 (3.15%)	0.19 (15.16%)	2.26%
7	0.591km - 3.365km	2.34375s	9,582 (7.57%)	0.55 (43.86%)	-17.7%
				Total 1.26	Overall 79.67%

(a)

Hierarchical Time-stepping by ClusterTech

Table | Chart | Segments

Level	Resolution distance between cells	Time step	#cell (%)	CPU core resource in giga cell-step per simulation day (%)	Saving
0	43.501km - 65.407km	150.000s	151,445 (18.12%)	0.11 (1.68%)	93.66%
1	20.782km - 51.632km	75.000s	19,391 (2.32%)	0.04 (0.59%)	82.75%
2	9.816km - 24.059km	37.500s	60,311 (7.22%)	0.21 (3.16%)	70.15%
3	4.786km - 11.333km	18.750s	178,131 (21.32%)	1.13 (17.18%)	45.02%
4	2.380km - 5.659km	9.375s	426,308 (51.02%)	5.08 (77.39%)	-3.46%
				Total 6.57	Overall 31.79%

(b)

Figure 5: HTS table listing the resolutions, time-steps, number of cells, and theoretical computational resources saving of each HTS levels for (a) the customized 128-to-1 km mesh and (b) the standard 60-to-3 km mesh

C. Estimation of required resources

In real simulations, the computational resource is mainly spent on integration for cells in time. The computational load of physics modules and I/O also grow with the number of cells. Taking approximation and for simplicity, we define a unit, 'Giga cell-step per simulation day' abbreviated as 'Gcs/day' to quantify the theoretical computational cost associated with a mesh for real simulations. This measure of computational cost is provided in the Mesh Generation Report for each mesh generated by CPAS. The computational cost for the standard 60-to-3 km mesh and customized 128-to-1 km mesh are 6.57 Gcs/day and 1.26 Gcs/day respectively.

3. Model and Hardware Configurations

In this study, CPAS version 0.4.0 was used to evaluate the efficiency of the meshes. The code was compiled and run using single-precision floating point calculations. The diagnostic variables were outputted in 3-hour interval using netCDF-4 format. The split dynamics include 2 sub-steps and 3 split steps, and the radiation scheme was called in 30-minute interval.

The cases and initial conditions used are identical to [8], in which cases 1 to 3 were respectively initialized on UTC 00 5 Jan 2018, UTC 00 11 Jun 2018 and UTC 00 12 Sep 2018 using The European Centre for Medium-Range Weather Forecasts ERA-Interim (0.75°×0.75°) [9]. The length of simulations were 5.5-day, where the first 12-hour was regarded as spin-up. The time-steps

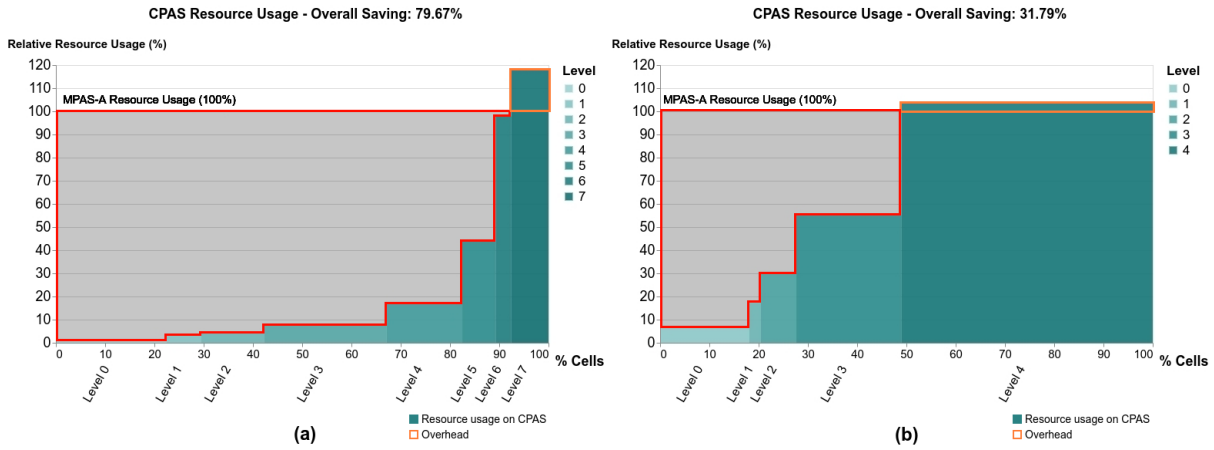

Figure 6: Graphical representation of Fig. 5 for (a) the customized 128-to-1 km mesh and (b) the standard 60-to-3 km mesh. The resource usage for simulation using the same mesh with (CPAS) and without HTS (MPAS-A) are respectively highlighted by the area of green bars and area under 100% resource usage. The area enclosed by the orange rectangle is the overhead. The overall resource saved by HTS is the difference of red region and orange rectangle.

used for HTS (and non-HTS) in the standard 60-to-3 km mesh and customized 128-to-1 km mesh are 150 s to 9.375 s (uniform 9.375 s) and 300 s to 2.3475 s(uniform 2.34375 s) respectively.

The Moderate Resolution Imaging Spectroradiometer (MODIS) was used as the land use classification. The topographical data was obtained from Global Multi-resolution Terrain Elevation Data 2010 (GMTED2010). The model was configured with 55 vertical levels, with the model top set to 30 km. The default physics suite on MPAS-A was adopted for all simulations, where the convective parameterization scheme was switched off by CPAS scale-aware feature for mesh cells smaller than 9 km (Table 1).

Table 1: The set of physics parameterization schemes used in this study

Parameterizations	Schemes
Convection	New Tiedtke [10] (switched off below 9 km)
Microphysics	WSM 6-class [11]
Land surface	Noah [12]
Boundary layer	YSU [13]
Surface layer	Monin-Obukhov [14]
Long Wave Radiation	RRTMG [15]
Short Wave Radiation	RRTMG [15]

All cases were run on the same set of computing nodes configuring Intel's Knights Landing processor (KNL). 4 KNL nodes with each containing 68 physical processors were used. The meshes were decomposed into 272 partitions, matching the same number of total physical cores, such that only one task was distributed to each processor. The MPI runs were boosted by setting `OMP_NUM_THREADS=4` and `OMP_STACKSIZE=128M`.

4. Results and Discussion

A. Efficiency Evaluation

Figure 7 shows the average timing profiles of some MPAS-A routines for the customized 128-to-1 km mesh and standard 60-to-3 km mesh over 3 historical cases. The results for HTS and non-HTS are respectively highlighted in magenta and dark-green for both figures. It is noted that, the component '`physics driver`' considers all physical parameterization procedures listed in Table 1 except microphysics.

Define speedup as:

$$S_{\text{latency}} = \frac{L_{\text{non-HTS}}}{L_{\text{HTS}}} \tag{5}$$

where $L_{\text{non-HTS}}$ and L_{HTS} refer to the execution time of non-HTS case and HTS case of the corresponding routine respectively.

It is observed that HTS boosts every major component in CPAS dynamic core in all cases using both standard and customized meshes, resulting in considerable speedup when compared to non-HTS. Refer to the profile for 128-to-1 km mesh in Fig. 7(a), speedup higher than 1.91x are recorded in routines '`microphysics`' and '`atm_advance_acoustic_step`', and speedup higher than 2.01x and 2.45x are recorded in '`atm_compute_dyn_tend`' and '`physics driver`' respectively in all three cases. Next, refer to the profile for 60-to-3 km mesh in Fig. 7(b), speedup of roughly 1.50x are recorded in all three cases for routines '`atm_compute_solve_diagnostics`', '`atm_advance_acoustic_step`' and '`atm_recover_large_step_variables`'.

The average total run time for the 128-to-1 km mesh is 33.4 hours (HTS) and 77.5 hours (non-HTS), resulting in 56.8% of average time saving (2.33x speedup) for HTS cases. In comparison, the average total run time for the 60-to-3 km mesh is 67.4 hours (HTS) and 80.7 hours (non-HTS). Therefore, the average time saving for HTS is 16.5% (1.20x speedup). Both cases have roughly half of the theoretical computational cost time saving shown in Fig. 5(a).

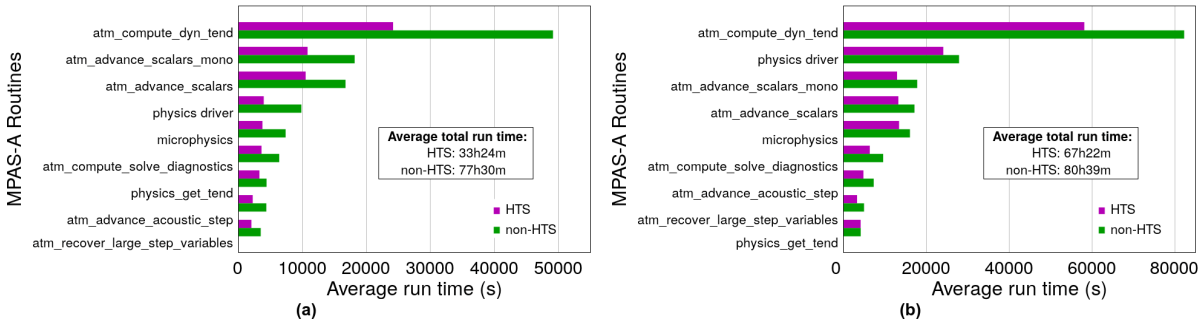

Figure 7: Average timing profile of the MPAS-A routines between HTS (magenta) and non-HTS (dark-green): (a) the customized 128-to-1 km mesh (b) the standard 60-to-3 km mesh

The time saving is particularly noteworthy for the 128-to-1 km mesh than the 60-to-3 km mesh. This result is consistent with the estimation depicted in Fig. 6, where the total area of the green bars in Fig. 6(b) is obviously smaller than that in Fig. 6(a). In other words, the time saved by HTS greatly depends on the resolution variation (or no. of HTS levels) as well as the distribution of cell sizes (or the 'Giga cell-step').

B. Predictability Evaluation

I. Comparison with FNL reanalysis data

Following the approach in [8], the model results were validated through comparison with the National Centers for Environmental Prediction (NCEP) Final (FNL) Operational Global Analysis. The FNL reanalysis data was prepared by ingesting surface observations, balloon data, wind profiler data, aircraft reports, buoy observations, radar observations and satellite observations. The model data in a 6-hour interval was interpolated to a 0.25°x0.25° regular lat-long grid before validation, matching the spatiotemporal resolution in FNL [16]. Various forecast variables - including mslp, t2m, q2, u10, v10, t850, q850, hgt500, u200 and v200 - over the 5-day analysis within the area of interest (a lat-long box covering 3 km refinement region of the MPAS-A 60-to-3 km mesh shown in Fig. 8) were extracted. The Taylor's skill scores were then computed following the equation mentioned in [8].

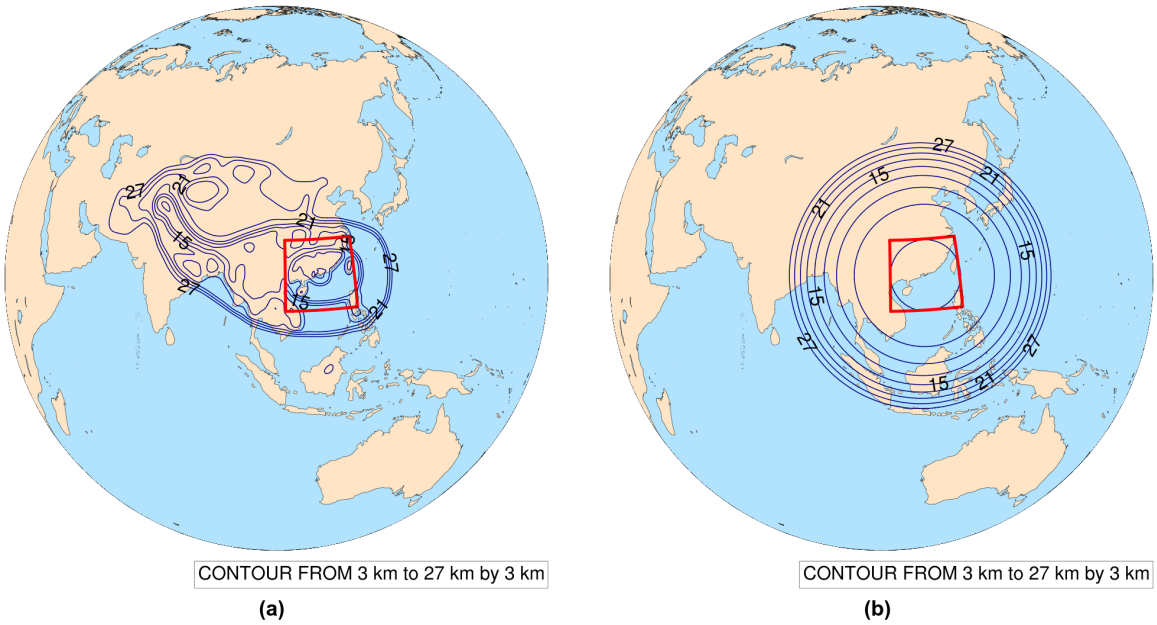

Figure 8: The model data within the red lat-long box, consisting of 61 (meridian) x 65 (zonal) grids, were extracted before comparison with FNL reanalysis data: (a) the customized 128-to-1 km mesh and (b) the standard 60-to-3 km mesh

The Taylor's skill scores are illustrated in the panel plot in Fig. 9, where the left column shows the customized 128-to-1 km mesh (i.e. Figs. 9(a), 9(c) and 9(e)) and the right column shows the standard 60-to-3 km mesh (i.e. Figs. 9(a), 9(d) and 9(f)). The top, middle and bottom figures respectively show results obtained for cases 1-3. It is observed that all forecast variables in the 5-day simulation show comparable performance in all cases with and without HTS for both customized and standard meshes, indicating the validity of the CPAS customized mesh running in HTS.

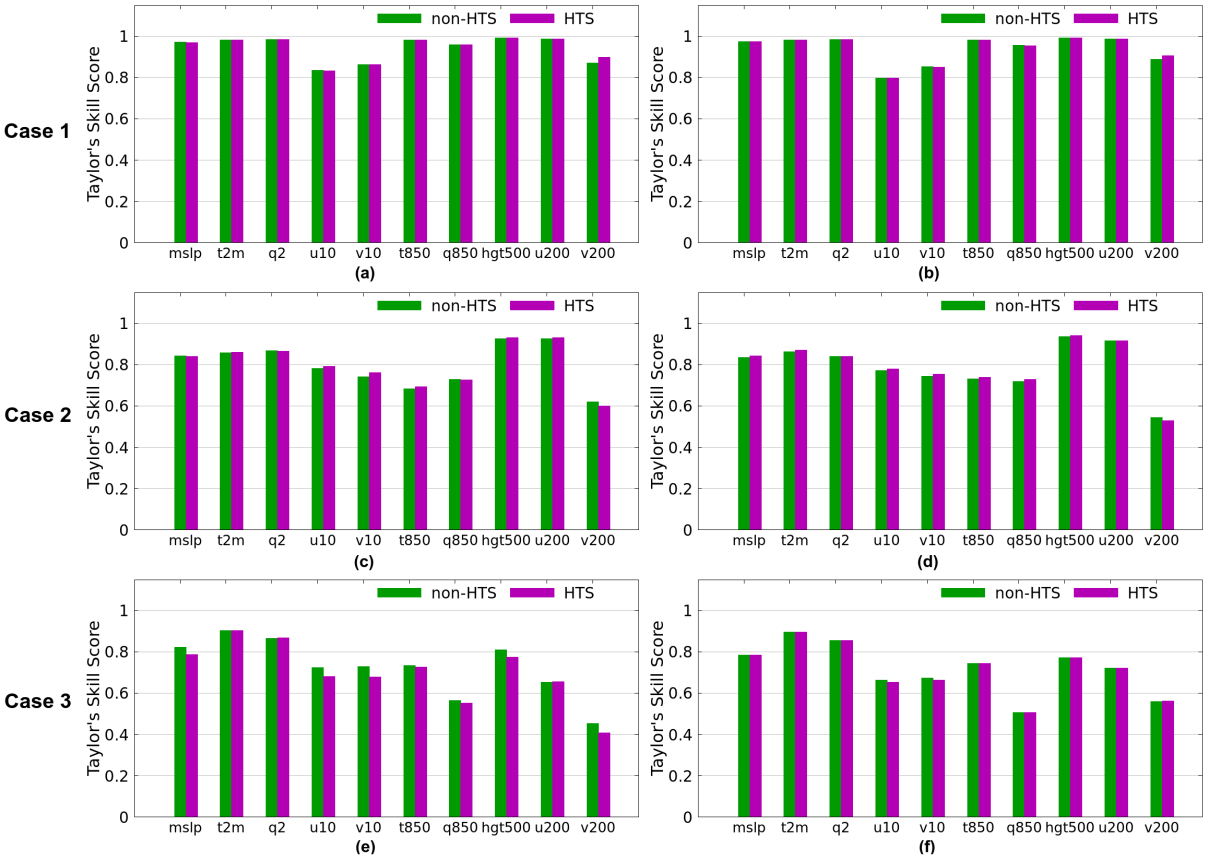

Figure 9: The Taylor's skill scores of the forecast variables between HTS and non-HTS for comparison with FNL reanalysis. (a), (c) and (e): Customized 128-to-1 km mesh for cases 1-3; (b), (d) and (f): standard 60-to-3 km mesh for cases 1-3

II. Comparison with HKO weather stations

To evaluate the simulation results in the high resolution region, i.e. the Hong Kong territories, the model data was compared against 28 HKO weather station observations (Fig. 10).

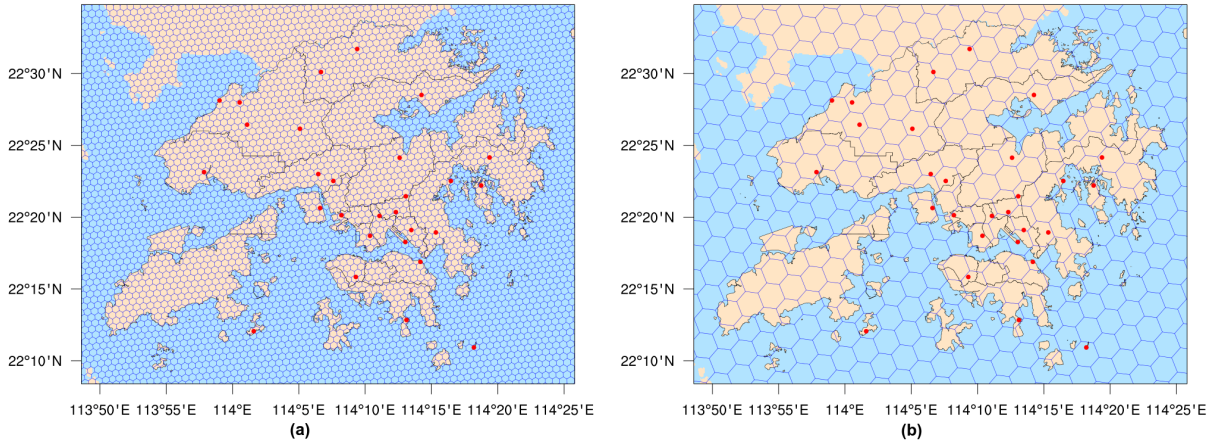

Figure 10: Geographic locations (red dots) of the 28 HKO stations for model evaluation, and the voronoi mesh for (a) the customized 128-to-1 km mesh and (b) the standard 60-to-3 km mesh

The model data, temperature at 2 meter ('t2m'), in the nearest cell in the mesh from each weather station was extracted. It is noteworthy that the distances from the cell centers to the stations are generally much shorter in the 128-to-1 km mesh than in the standard 60-to-3km mesh, because the former is customized to have 1 km resolution over this region of interest. 3-hourly CPAS output data are aggregated into daily average temperature to match to the available daily observation data. Scatter plots are made and the correlation (r), mean absolute error (MAE) and root-mean-square error (RMSE) for both customized and standard meshes were computed (Fig. 11). Furthermore, the plot of Taylor's skill scores for all simulation runs are shown in Fig. 12.

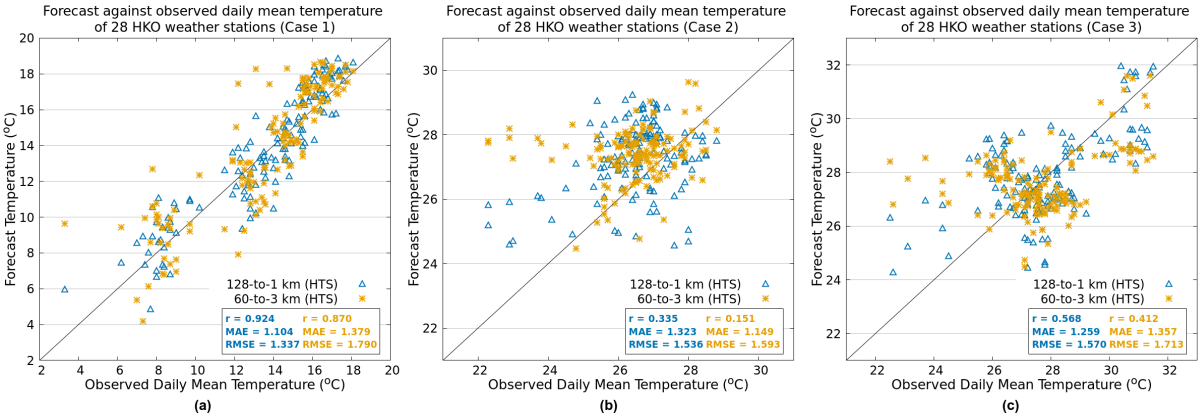

Figure 11: Scatter plots for averaged forecast temperature against observed daily mean temperature of 28 HKO weather stations (a)-(c): Cases 1-3

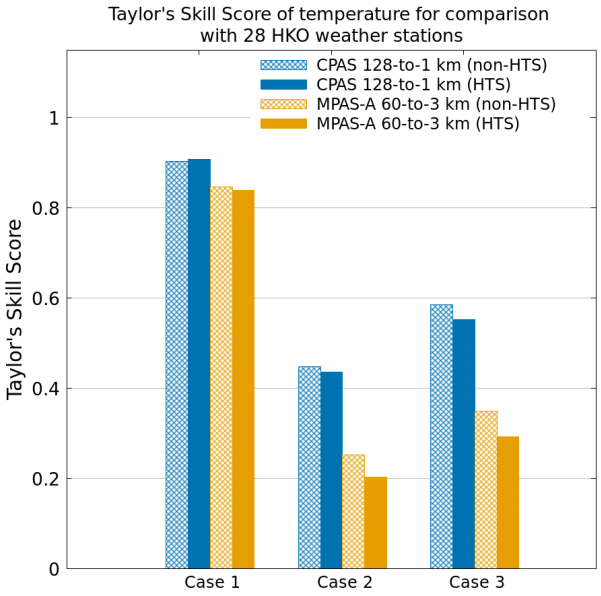

Figure 12: The Taylor's skill scores of temperature for comparison with 28 HKO weather stations

Refer to Fig. 11, the customized 128-to-1 km mesh (blue triangles) generally produces higher correlation, smaller MAE, and smaller RMSE than the standard 60-to-3 km mesh (yellow stars) in all cases, except a larger MAE is found in case 2 (Fig. 11(b)). These results provide an insight of using high resolution meshes up to 1 km in real simulations. As CPAS supports multi-resolution static data as input, higher resolution static data – including soil type, topographical data and landuse data – were used in high resolution regions. This plays an important role on how the static fields are represented in the model, particularly in resolving the topography and land-water boundaries. For instance, for a weather station located in the coastal area, a lower resolution mesh (even for high resolution static source data) might possibly misinterpret the surface as sea.

5. Conclusion

The efficiency of the customized 128-to-1 km mesh and standard 60-to-3 km mesh with and without HTS are evaluated by running three cases using the same model settings. The run time of all MPAS-A routines for HTS simulations are significantly shorter than that for non-HTS in all cases. On average, the real time saving for the customized 128-to-1 km mesh and standard 60-to-3 km mesh are 56.8% (2.33x speedup) and 16.5% (1.20x speedup) respectively. The promising model performance along with remarkable speedup indicate the validity and feasibility of high resolution local/regional forecast using customized global variable-resolution meshes in an operational manner.

Acknowledgement

The daily mean temperature data of 28 HKO weather stations is obtained from the OpenData API of the Hong Kong Government.

Technical reference about the daily mean temperature data:
`https://data.weather.gov.hk/weatherAPI/doc/HKO_Open_Data_API_Documentation.pdf`
(p. 13 and p.18, dataType: CLMTEMP)

Source of the Materials:
`https://www.hko.gov.hk`

References

[1] R. L. Walko and R. Avissar, "A direct method for constructing refined regions in unstructured conforming triangular–hexagonal computational grids: Application to OLAM," *Monthly Weather Review*, vol. 139, no. 12, pp. 3923–3937, 2011. [Online]. Available: https://doi.org/10.1175/MWR-D-11-00021.1

[2] ——, "The Ocean–Land–Atmosphere Model (OLAM). Part I: shallow-water tests," *Monthly Weather Review*, vol. 136, no. 11, pp. 4033–4044, 2008. [Online]. Available: https://doi.org/10.1175/2008MWR2522.1

[3] ——, "The Ocean–Land–Atmosphere Model (OLAM). Part II: Formulation and tests of the nonhydrostatic dynamic core," *Monthly Weather Review*, vol. 136, no. 11, pp. 4045–4062, 2008. [Online]. Available: https://doi.org/10.1175/2008MWR2523.1

[4] H. Weller, H. G. Weller, and A. Fournier, "Voronoi, Delaunay, and block-structured mesh refinement for solution of the shallow-water equations on the sphere," *Monthly Weather Review*, vol. 137, no. 12, pp. 4208–4224, 2009. [Online]. Available: https://doi.org/10.1175/2009MWR2917.1

[5] T. D. Ringler, D. Jacobsen, M. Gunzburger, L. Ju, M. Duda, and W. Skamarock, "Exploring a multiresolution modeling approach within the shallow-water equations," *Monthly Weather Review*, vol. 139, no. 11, pp. 3348–3368, 2011. [Online]. Available: https://doi.org/10.1175/MWR-D-10-05049.1

[6] D. Engwirda, "JIGSAW-GEO (1.0): locally orthogonal staggered unstructured grid generation for general circulation modelling on the sphere," *Geoscientific Model Development*, vol. 10, no. 6, pp. 2117–2140, 2017. [Online]. Available: https://www.geosci-model-dev.net/10/2117/2017/

[7] M. Duda, L. Fowler, B. Skamarock, C. Roesch, D. Jacobsen, and T. Ringler, "Mpas-atmosphere model user's guide version 6.0," 2018. [Online]. Available: http://www2.mmm.ucar.edu/projects/mpas/mpas_atmosphere_users_guide_6.0.pdf

[8] ClusterTech Ltd, "Forecast skill analysis for hierarchical time-stepping on cpas," 2019. [Online]. Available: https://cpas.earth/support/download/

[9] D. P. Dee, S. M. Uppala, A. J. Simmons, P. Berrisford, P. Poli, S. Kobayashi, U. Andrae, M. A. Balmaseda, G. Balsamo, P. Bauer, P. Bechtold, A. C. M. Beljaars, L. van de Berg, J. Bidlot, N. Bormann, C. Delsol, R. Dragani, M. Fuentes, A. J. Geer, L. Haimberger, S. B. Healy, H. Hersbach, E. V. Hólm, L. Isaksen, P. Kållberg, M. Köhler, M. Matricardi, A. P. McNally, B. M. Monge-Sanz, J.-J. Morcrette, B.-K. Park, C. Peubey, P. de Rosnay, C. Tavolato, J.-N. Thépaut, and F. Vitart, "The ERA-Interim reanalysis: configuration and performance of the data assimilation system," *Quarterly Journal of the Royal*

Meteorological Society, vol. 137, no. 656, pp. 553–597, 2011. [Online]. Available: https://rmets.onlinelibrary.wiley.com/doi/abs/10.1002/qj.828

[10] C. Zhang and Y. Wang, "Projected future changes of tropical cyclone activity over the western north and south pacific in a 20-km-mesh regional climate model," *Journal of Climate*, vol. 30, no. 15, pp. 5923–5941, 2017. [Online]. Available: https://doi.org/10.1175/JCLI-D-16-0597.1

[11] S. Y. Hong, "The WRF single-moment 6-class microphysics scheme (WSM6)," *J. Korean Meteor. Soc.*, vol. 42, pp. 129–151, 2006. [Online]. Available: https://ci.nii.ac.jp/naid/10024028200/en/

[12] M. Tewari, F. Chen, W. Wang, J. Dudhia, M. A. LeMone, K. Mitchell, M. Ek, G. Gayno, J. Wegiel, and R. H. Cuenca, "Implementation and verification of the unified NOAH land surface model in the WRF model," *20th conference on weather analysis and forecasting/16th conference on numerical weather prediction*, pp. 11–15, 2004.

[13] S. Y. Hong, Y. Noh, and J. Dudhia, "A new vertical diffusion package with an explicit treatment of entrainment processes," *Monthly Weather Review*, vol. 134, no. 9, pp. 2318–2341, 2006. [Online]. Available: https://doi.org/10.1175/MWR3199.1

[14] Z. I. Janjic, "Nonsingular implementation of the Mellor-Yamada level 2.5 scheme in the NCEP meso model," *NCEP Office Note*, no. 437, p. 61, 2002.

[15] M. Iacono, J. Delamere, E. Mlawer, M. Shephard, S. Clough, and W. Collins, "Radiative forcing by long-lived greenhouse gases: Calculations with the AER radiative transfer models," *Journal of Geophysical Research: Atmospheres*, vol. 113, no. D13, 2008. [Online]. Available: https://agupubs.onlinelibrary.wiley.com/doi/abs/10.1029/2008JD009944

[16] NCEP, "NCEP GDAS/FNL 0.25 Degree Global Tropospheric Analyses and Forecast Grids," Boulder CO, 2015. [Online]. Available: https://doi.org/10.5065/D65Q4T4Z

